Society of Medical Education & Research

2026, Volume 6, Issue 1, Page No: 1-20
ISSN: 3108-4834

Archive of International Journal of Cancer and Allied Science

Mechanistic Insights into miR-23a/27a/24-2 Cluster-Mediated Tumor Immune Evasion and Resistance to Immune Checkpoint Blockade in Non-Small Cell Lung Cancer

Pieter Botha[1]*, Anel Van Wyk[1], Johan Marais[2]

[1]Department of NSCLC Immunotherapy and miRNA Biology, Faculty of Medicine, Stellenbosch University, Stellenbosch, South Africa.
[2]Department of Immune Evasion and Checkpoint Resistance, Faculty of Medicine, University of Pretoria, Pretoria, South Africa.

***E-mail** ✉ pieter.botha@sun.ac.za

Abstract

Programmed death-ligand 1 (PD-L1) and major histocompatibility complex class I (MHC-I) play central roles in enabling tumors to evade immune surveillance and in conferring resistance to PD-1/PD-L1 inhibitors. The present work demonstrates that increased expression of all members of the miR-23a/27a/24−2 cluster is associated with reduced patient survival, heightened immune escape, and diminished responsiveness to PD-1/PD-L1 blockade in individuals with non-small cell lung cancer (NSCLC). Forced expression of these cluster miRNAs promoted PD-L1 production through direct suppression of Cbl proto-oncogene B (CBLB). It concurrently lowered MHC-I levels by elevating eukaryotic initiation factor 3B (eIF3B) via inhibition of microphthalmia-associated transcription factor (MITF). We further established that sustained expression of the miR-23a/27a/24−2 cluster in NSCLC cells is supported by augmented Wnt/β-catenin pathway activity, which strengthens the binding of transcription factor 4 (TCF4) to the cluster's promoter region. Pharmacological interference with eIF3B signaling markedly improved the efficacy of PD-1/PD-L1 blockade therapy, particularly in NSCLC tumors with high levels of the miR-23a/27a/24−2 cluster. This improvement resulted from restored MHC-I surface expression while preserving the elevated PD-L1 induced by the miRNA cluster. Overall, this study clarifies the self-reinforcing loop that maintains miR-23a/27a/24−2 cluster activity and reveals the detailed molecular processes through which these miRNAs drive immune evasion and therapeutic resistance. These insights also identify a targeted intervention strategy for managing NSCLC cases characterized by strong expression of the miR-23a/27a/24−2 cluster.

Keywords: Non-small cell lung cancer, miR-23a/27a/24-2 cluster, Tumor immune evasion, Immune checkpoint blockade, PD-L1, MHC-I

Introduction

Lung cancer is the most frequently diagnosed cancer and the foremost cause of cancer mortality across the world [1]. Non-small cell lung cancer (NSCLC) accounts for roughly 85% of all lung cancer diagnoses and represents its most common form [2]. Although recent therapeutic progress has been made, long-term survival remains limited, with fewer than 20% of NSCLC patients alive five years after diagnosis [2, 3]. Growing research underscores immune evasion as a fundamental driver of tumor advancement and a major impediment to effective cancer treatment [4]. As a result, immune checkpoint blockade (ICB) has gained prominence as a valuable treatment option for various malignancies, including NSCLC, yielding notable clinical benefits in many cases [3, 5]. Nonetheless, durable responses are achieved in only a minority of patients receiving ICB, whether used alone or combined with chemotherapy [3, 6]. A deeper insight into the processes governing tumor immune

Access this article online https://smerpub.com/

Received: 06 October 2025; **Accepted:** 08 January 2026

How to cite this article: Botha P, Van Wyk A, Marais J. Mechanistic Insights into miR-23a/27a/24-2 Cluster-Mediated Tumor Immune Evasion and Resistance to Immune Checkpoint Blockade in Non-Small Cell Lung Cancer. Arch Int J Cancer Allied Sci. 2026;6(1):1-20. https://doi.org/10.51847/PZ3cesSrWh

escape and ICB resistance is therefore indispensable for designing improved treatment approaches.

Multiple molecular regulators, particularly microRNAs (miRNAs), modulate tumor immune evasion. MiRNA clusters are especially potent because their individual members can simultaneously repress the same target or distinct genes within a shared pathway, producing cooperative effects [7, 8]. The miR-23a/27a/24−2 cluster consists of miR-23a, miR-27a, and miR-24-2. Earlier work from our group showed that these miRNAs are overexpressed in early-stage NSCLC, where they accelerate disease recurrence after surgery by stimulating Wnt/β-catenin signaling [9]. Activation of this pathway is known to facilitate immune escape and reduce sensitivity to ICB in NSCLC [10]. In addition, the miR-23a/27a/24−2 cluster has been reported to impair interferon-γ (IFN-γ) production and antigen-driven cytotoxicity in CD8+ T lymphocytes [11]. Based on these observations, we postulated that upregulation of the miR-23a/27a/24−2 cluster contributes significantly to immune evasion and resistance to PD-1/PD-L1 blockade in NSCLC.

The present study establishes that elevated levels of the miR-23a/27a/24−2 cluster of miRNAs correlate closely with immune evasion and resistance to PD-1/PD-L1 blockade in NSCLC. Experimental findings revealed that these miRNAs strongly inhibit IFN-γ release from T cells, limit CD8+ T cell infiltration within tumors, reduce MHC-I expression, and increase PD-L1 abundance on NSCLC cells. At the mechanistic level, the cluster miRNAs enhance PD-L1 expression by suppressing its negative regulator Cbl proto-oncogene B (CBLB). At the same time, they decrease MHC-I by increasing eukaryotic initiation factor 3B (eIF3B) protein levels by repressing the upstream negative regulator microphthalmia-associated transcription factor (MITF). We also determined that the miR-23a/27a/24−2 cluster sustains its own high expression by activating Wnt/β-catenin signaling, which in turn promotes greater association of transcription factor 4 (TCF4) with the cluster promoter. Finally, pharmacological inhibition of either the eIF3B pathway or the β-catenin/TCF4 axis substantially enhanced the antitumor efficacy of PD-1/PD-L1 blockade in NSCLC tumors with high cluster miRNA expression, with eIF3B-targeting demonstrating superior therapeutic benefit.

Materials and Methods

Human samples and cell culture

Peripheral blood samples were drawn from 20 healthy volunteers to obtain peripheral blood mononuclear cells (PBMCs). Tumor tissues from 82 NSCLC patients were also collected during surgical procedures or biopsies at Daping Hospital, and the study protocol received approval from the relevant ethics committees. All cell lines utilized in this investigation were acquired from the Shanghai Cell Bank of the Chinese Academy of Sciences (Shanghai, China). Both 293T and Lewis lung cancer (LLC) cells were grown in Dulbecco's modified Eagle's medium supplemented with 10% fetal bovine serum (FBS) (HyClone, Logan, UT). H1299 and H1650 cells were maintained in RPMI1640 medium containing 10% FBS.

Constructs

Plasmids encoding MITF (EX-B5124-M35), CBLB (EX-Z7996-M35), and eIF3B shRNA (HSH066232), together with their respective control empty or scrambled vectors, were obtained from iGene Biotechnology Co., Ltd. (Guangzhou, China). The β-catenin overexpression construct (HG11279-CF) was sourced from Sino Biological Inc. (Beijing, China). Vectors for expression of the miR-23a/27a/24−2 cluster and the corresponding shRNA or scramble controls were purchased from Genechem Co. Ltd. (Shanghai, China). For the miRNA luciferase reporter experiments, the 3′-untranslated regions (3′-UTRs) of CBLB and MITF were PCR-amplified from cDNA prepared from normal human lung tissue RNA and subcloned into the MluI and HindIII sites of the pMIR-REPORT™ miRNA expression reporter vector (Thermo Fisher Scientific, Waltham, MA, USA). For promoter activity assays, the promoter region of the miR-23a/27a/24−2 cluster was amplified from human genomic DNA and ligated into the NheI and BglII sites of the pGL4.10 luciferase reporter vector (Promega, Madison, WI, USA).

Co-culture of T cells and tumor cells

PBMCs were separated from fresh blood of healthy donors using lymphocyte separation medium as specified by the manufacturer (Tianjin Hao Yang Biological Manufacture Co., Ltd., Tianjin, China). Activation of immune cells was performed following a previously published protocol [12]. CD8+ T cells were subsequently isolated using a CD8+ T cell isolation kit (Miltenyi Biotec) according to the manufacturer's instructions.

Assessment of T cell-induced tumor cell killing was performed as previously described [12]. In short, NSCLC cells were transfected with either empty vector or miR-23a/27a/24−2 cluster expression plasmids. Forty-eight hours later, these cells were incubated with pre-activated T cells at an effector-to-target ratio of 1:20 for 6 hours, and the extent of cell death was evaluated using flow cytometry.

CD8+ T cell chemotaxis was examined using a transwell migration assay as described by Shang *et al*. [13]. NSCLC cells were transfected with a control vector or with constructs overexpressing the miR-23a/27a/24−2 cluster. After 48 hours, the medium was refreshed, and following another 48-hour incubation period, the conditioned medium was placed in the lower compartment of the transwell insert. Activated CD8+ T cells (5×10^5 cells in 100 μl), pre-labeled with anti-human CD8α APC-Cy7 antibody (Invitrogen, Cat#: A15448), were then added to the upper chamber. Following a 2-hour incubation, migrated cells in the lower chamber were counted by flow cytometry.

The influence of miR-23a/27a/24−2 cluster-overexpressing NSCLC cells on interferon-gamma (IFN-γ) release from T cells was tested by transfecting NSCLC cells with the appropriate constructs. Forty-eight hours post-transfection, the cells were co-incubated with activated T cells at a 1:10 ratio for 12 hours. Culture supernatants were collected, and IFN-γ levels were determined using a human IFN-γ ELISA kit (Invitrogen) according to the manufacturer's recommendations.

Luciferase reporter assay

In miRNA target validation assays, 293T cells were transfected with firefly luciferase reporters harboring the 3′-UTR sequences of either CBLB or MITF, followed by introduction of miR-23a/27a/24−2 cluster expression vectors or control plasmids. For promoter reporter experiments, 293T cells carrying the firefly luciferase construct driven by the miR-23a/27a/24−2 cluster promoter were transfected with TCF4 or β-catenin expression plasmids, or their respective empty vectors. A Renilla luciferase plasmid served as an internal control for transfection efficiency in all cases. Cells were harvested 72 hours after transfection, and luciferase activities were quantified using the Dual-Luciferase Assay Kit (Promega).

Western blot (WB), immunohistochemistry (IHC), immunofluorescence (IF), and co-immunoprecipitation (Co-IP) assay

Western blotting, immunohistochemical analysis, immunofluorescence staining, and co-immunoprecipitation were performed according to protocols reported in prior studies [14]. Band densities on Western blots were quantified using ImageJ. Immunohistochemical staining was scored independently by two blinded pathologists. The primary antibodies employed included those directed against eIF3B (Cat No: bs-14542R, Lot No: BC12254757; for IHC), MITF (Cat No: bsm-51339 M, Lot No: BD06051693), MHC-I (Cat No: bs-18070R, Lot No: BD07151765 for WB; bs-2355R, Lot No: BD07151765 for IHC and IF), and PD-L1 (Cat No: bs-22022R, Lot No: BD7153735 for flow cytometry), all supplied by Beijing Biosynthesis Biotechnology Co., Ltd (Beijing, China). Antibodies recognizing β-catenin (Cat No: 8480 S, Lot No: 5), Histone H3 (Cat No: 9715 S, Lot No: 20), and Actin (Cat No: 4970 S, Lot No: 20) were obtained from Cell Signaling Technology (Danvers, MA, USA). Anti-CD8 antibodies (Cat No: ab217344, Lot No: 00121531; Cat No: ab17147, Lot No: 3258634-5) and anti-PD-L1 antibody (Cat No: ab279292, Lot No: 1007824-2 for WB) were acquired from Abcam (Cambridge, MA, USA). Additional antibodies against CBLB (Cat No: 66353-1, Lot No: 10003654), TCF4 (Cat No: 22337-1-AP, Lot No: 00121531), eIF3B (Cat No: 68202-1, Lot No: 10028876 for WB), and PD-L1 (Cat No: 66248-1, Lot No: 10022147 for IHC) were provided by Proteintech (Wuhan, Hubei, China). Control rabbit IgG (Cat No: 30000-0-AP, Lot No: 00140749) and mouse IgG (Cat No: BS-0296P, Lot No: BC06261797) were sourced from Proteintech and Beijing Biosynthesis Biotechnology Co., Ltd, respectively.

Real-time quantitative reverse transcriptase polymerase chain reaction (qRT-PCR) and miRNA in situ hybridization (ISH)

Total RNA was extracted using TRIzol reagent (Beyotime, Shanghai, China). Transcript levels were quantified by qRT-PCR using the SYBR Green One-Step qRT-PCR kit (Beyotime Biotechnology) according to the manufacturer's recommendations. Specific primers for U6, hsa-miR-23a, hsa-miR-24-2, and hsa-miR-27a were obtained from GeneCopoeia (Rockville, MD, USA). miRNA quantification was conducted with the All-in-One™ miRNA qRT-PCR detection kit 2.0

(GeneCopoeia) following the supplier's protocol. miRNA expression data were normalized relative to U6 snRNA.

In situ hybridization for miRNAs and subsequent scoring followed the approaches outlined by Nuovo [15] and Guo *et al*. [16]. Paraffin-embedded tissue sections were deparaffinized, and antigen retrieval was conducted by boiling in citrate buffer for 15 minutes. Sections were then digested with proteinase K for 15 minutes and pre-hybridized in appropriate buffer for 1 hour at 37 °C. Hybridization was performed overnight at 37 °C in buffer containing probes specific for miR-23a, miR-24-2, or miR-27a, with probe-free buffer serving as a negative control. Custom miRNA probes were synthesized by Zoonbio Biotechnology Co., Ltd (Nanjing, China).

RNA sequencing and proteomics analysis

Shanghai Genechem Co., Ltd. performed RNA sequencing and downstream data analysis according to the workflow described by Li *et al*. [17]. In summary, RNA libraries for Illumina sequencing were generated using the NEBNext Ultra RNA Library Prep Kit and sequenced on the NovaSeq platform. Raw FASTQ reads were pre-processed with custom Perl scripts. Alignment to the reference genome was performed with HISAT2, incorporating splice junction information from the provided gene annotation file.

Proteomics experiments were completed as previously detailed [18]. Briefly, H1299 cells were transfected with either the miR-23a/27a/24−2 cluster expression plasmid or control vector. Seventy-two hours later, proteins were isolated and denatured. Digested peptides were labeled using iTRAQ reagents and separated by reversed-phase fractionation on an Agilent 1260 Infinity II HPLC system. Mass spectra were acquired on a Q-Exactive Plus instrument (Thermo Fisher Scientific) interfaced with an Easy-nLC system (Thermo Fisher Scientific). Raw data were processed and analyzed using Mascot 2.6 and Proteome Discoverer 2.1.

Electrophoretic mobility shift assay (EMSA)

Putative TCF4 binding motifs in the miR-23a/27a/24−2 cluster promoter were identified through the hTFtarget resource [19]. EMSA was performed using the LightShift Chemiluminescent EMSA Kit (Thermo Fisher Scientific) according to the manufacturer's guidelines and prior methodology [14].

Chromatin immunoprecipitation (ChIP)-qPCR assay

For ChIP-qPCR, 293T cells were transfected with a β-catenin expression plasmid or empty vector control. Forty-eight hours post-transfection, cells were treated with 1% formaldehyde at room temperature to cross-link proteins to DNA, and the reaction was terminated with glycine. Following lysis in ChIP buffer, chromatin was fragmented by sonication, precleared, and incubated overnight with 2 μg of anti-TCF4 antibody or control IgG. Immune complexes were captured with protein G/A agarose beads. After washing with low- and high-salt buffers, complexes were eluted at 65°C for 15 minutes. Cross-links were reversed by addition of NaCl (final concentration 0.2 M) and incubation overnight at 65°C. The recovered DNA was purified and analyzed by quantitative PCR.

Animal study

Female C57BL/6J mice and male SCID mice, both six weeks of age, were obtained from Beijing HFK Bioscience Co., Ltd (Beijing, China) for use in the in vivo experiments. The influence of the miR-23a/27a/24−2 cluster on immune evasion by lung cancer cells was assessed in syngeneic C57BL/6J and immunodeficient SCID xenograft tumor models. To generate the C57BL/6J model, 1×10^6 LLC cells transfected with a control empty vector, miR-23a/27a/24−2 cluster overexpression plasmid, scramble sequence, or cluster-specific shRNA were resuspended in 100 μl phosphate-buffered saline (PBS) and injected subcutaneously into the dorsal region of the mice. For the SCID xenograft model, 2×10^6 H1299 cells transfected with scramble control or shRNA directed against the miR-23a/27a/24−2 cluster in 100 μl PBS were implanted subcutaneously. Three days after tumor cell inoculation, mice were injected intravenously with 3×10^6 human PBMCs or vehicle control via the tail vein. Tumor size was measured weekly.

Investigation of the miR-23a/27a/24−2 cluster's role in resistance to PD-1/PD-L1 blockade was performed using C57BL/6J xenograft tumors. In these experiments, 1×10^6 LLC cells transfected with an empty vector or miR-23a/27a/24−2 cluster expression plasmid in 100 μl PBS were inoculated subcutaneously. Treatment commenced once tumors reached approximately 100 mm^3 in volume. Mice received PD-L1 monoclonal antibody at a dose of 1 mg/kg body weight or control rat IgG (Bio X Cell) every three days via intravenous administration.

The efficacy of combining LF3 with PD-1/PD-L1 blockade therapy in tumors expressing high levels of the

miR-23a/27a/24−2 cluster was tested in C57BL/6J xenografts established with LLC cells overexpressing the cluster, as described above. When tumors reached ~100 mm³, animals were randomly assigned to four treatment arms. The control arm received IgG, while the remaining groups received PD-L1 mAb monotherapy (1 mg/kg every three days), LF3 monotherapy (50 mg/kg every two days), or the dual combination of PD-L1 mAb plus LF3, all delivered intravenously.

To directly compare the adjuvant effects of LF3 and 4EGI-1 when paired with PD-1/PD-L1 blockade, additional C57BL/6J xenografts were generated using high miR-23a/27a/24−2 cluster-expressing LLC cells. Upon reaching a tumor volume of ~100 mm³, mice were randomized into three groups. One group was treated with PD-L1 mAb alone (1 mg/kg every three days), while the other two groups received PD-L1 mAb combined with either LF3 or 4EGI-1 (75 mg/kg body weight, administered intraperitoneally five days per week). All procedures involving animals adhered to the Army Medical University Policy on the Care and Use of Laboratory Animals.

Statistical analysis

Quantitative data are reported as mean ± standard deviation derived from a minimum of three independent replicates. Statistical analyses were performed using SPSS software, and differences were considered significant when $p < 0.05$.

Results and Discussion

High expression of miRNAs in the miR-23a/27a/24−2 cluster is strongly associated with disease progression and immune evasion in NSCLC

To determine the association between miR-23a/27a/24−2 cluster miRNA levels and NSCLC advancement, patients were categorized based on tumor-to-adjacent tissue expression ratios. Individuals showing elevated expression of all cluster miRNAs in tumor samples compared with paired normal tissues formed the high-expression cohort. Those with reduced or equivalent levels were placed in the low-expression cohort. Analysis of clinical records demonstrated that higher miR-23a/27a/24−2 cluster expression correlated with decreased overall survival **(Figure 1a)** and poorer disease-free survival **(Figure 1b)**. The high-expression group also exhibited significantly reduced infiltration of CD8+ T cells within tumor tissues **(Figure 1c)**. Gene Ontology (GO) pathway analysis performed on mRNA sequencing profiles from miR-23a/27a/24−2 cluster-silenced H1299 cells relative to controls highlighted pronounced effects on T cell activation and differentiation pathways **(Figure 1d)**. Gene set enrichment analysis (GSEA) confirmed a strong inverse relationship between cluster miRNA expression and T cell-mediated immune signatures in NSCLC cells **(Figure 1e)**. Similar patterns emerged from examination of the GEO dataset GSE151103, which likewise connected miR-23a/27a/24−2 cluster abundance to T cell activation and differentiation processes **(Figure 1f)**. Furthermore, target gene-based functional enrichment [20] linked these miRNAs to broad immune system regulatory functions **(Figure 1g)**. In summary, these observations support the conclusion that overexpression of the miR-23a/27a/24−2 cluster drives NSCLC progression primarily by attenuating T cell-mediated antitumor responses.

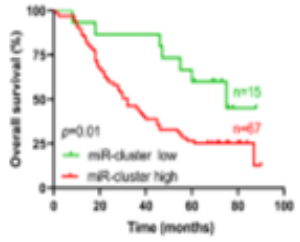

a)

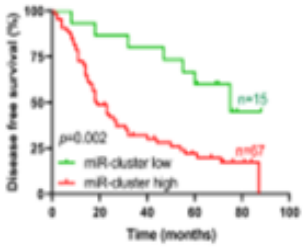

b)

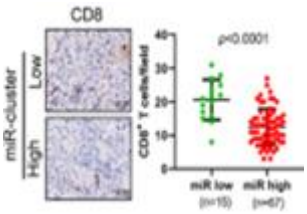

c)

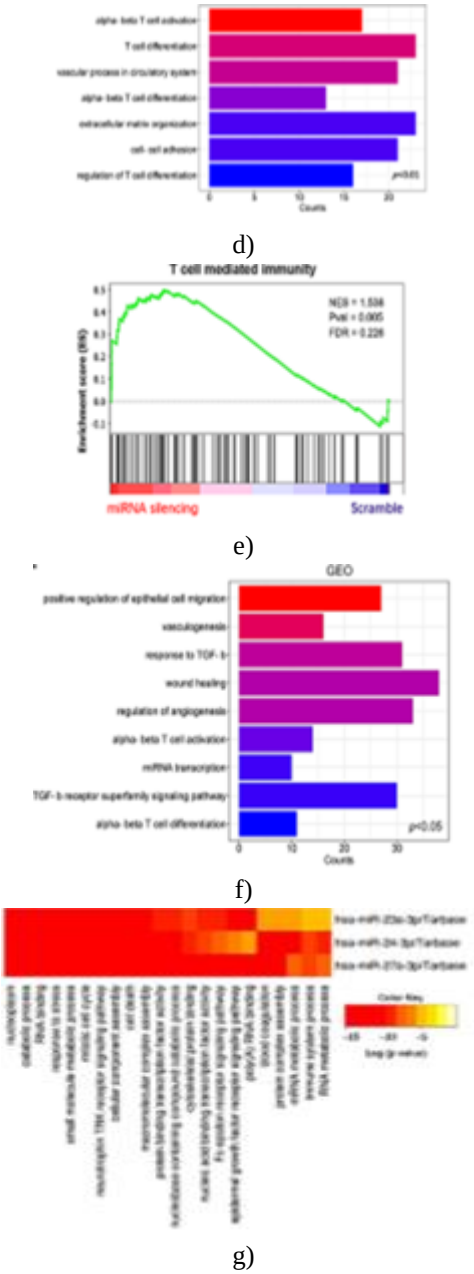

Figure 1. High expression of the miR-23a/27a/24−2 cluster is closely associated with an unfavorable disease course and tumor immune evasion in NSCLC

Kaplan-Meier curves showing shorter overall survival (a) and reduced disease-free survival (b) among NSCLC patients with high expression of the miR-23a/27a/24−2 cluster. Data were derived from a cohort of 82 patients, and statistical significance was assessed using the log-rank test. (c) Representative images of CD8 immunohistochemical staining and quantification of infiltrating CD8+ T cells in human NSCLC specimens (per 100 × 100 μm field). p-values were obtained using the t-test. (d) Gene Ontology (GO) enrichment analysis of mRNA sequencing data obtained from H1299 cells following miR-23a/27a/24−2 cluster knockdown versus control cells, (e) Gene Set Enrichment Analysis (GSEA) demonstrating negative enrichment of T cell-mediated immunity gene sets in association with miR-23a/27a/24−2 cluster expression. Analysis utilized mRNA sequencing data from silenced and control H1299 cells, (f) GO analysis conducted on GEO dataset GSE151103, and (g) Functional annotation based on predicted miRNA targets (http://www.microrna.gr/miRPathv4). miR-cluster, miR-23a/27a/24−2 cluster.

Overexpression of the miR-23a/27a/24−2 cluster in NSCLC inhibits the T-cell-mediated immune response

To examine the direct influence of miR-23a/27a/24−2 cluster-overexpressing NSCLC cells on T cell function, co-culture systems were established as illustrated, followed by comprehensive evaluation of T cell performance. Data showed that elevated expression of the miR-23a/27a/24−2 cluster in NSCLC cells markedly suppressed IFN-γ secretion from T cells **(Figure 2a)**, attenuated the cytotoxic activity of T cells against tumor targets **(Figure 2b)**, and impaired the migratory capacity of T cells **(Figure 2c)**.

The involvement of this miRNA cluster in promoting immune evasion was additionally explored in immunocompetent animal models utilizing Lewis lung cancer (LLC) cells. The LLC-C57BL/6J model is particularly appropriate for immune-related investigations since these cells can establish tumors in non-immunodeficient hosts [21]. Overexpression of all miRNAs within the miR-23a/27a/24−2 cluster in LLC cells resulted in accelerated tumor expansion **(Figure 2d)**, decreased accumulation of CD8+ T cells inside the tumors **(Figure 2e)**, and reduced IFN-γ production in the tumor milieu **(Figure 2f)**. In contrast, genetic silencing of the cluster restrained tumor development **(Figure 2g)**, promoted greater CD8+ T cell recruitment into neoplastic tissue **(Figure 2h)**, and elevated local IFN-γ levels **(Figure 2i)**.

Comparable outcomes were obtained in immunodeficient models. Knockdown of the miR-23a/27a/24−2 cluster in H1299 cells led to significant retardation of tumor progression in SCID mice, both in the presence **(Figure 2j)** and absence **(Figure 2l)** of human PBMC transfer. Cluster inhibition also enhanced CD8+ T cell infiltration when PBMCs were provided

(Figure 2k). Notably, reconstitution with PBMCs enhanced the antitumor effect of cluster silencing, resulting in a higher inhibition rate **(Figure 2m)**. Overall, these experiments demonstrate that the miR-23a/27a/24−2 cluster plays a substantial role in dampening T cell-dependent antitumor immunity within NSCLC.

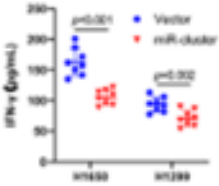

a)

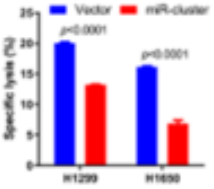

b)

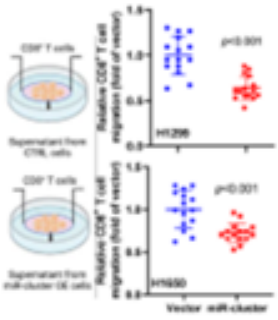

c)

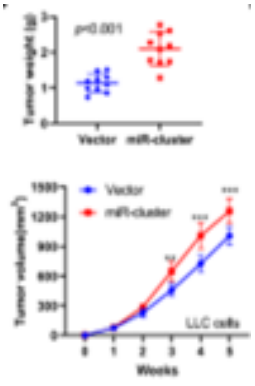

d)

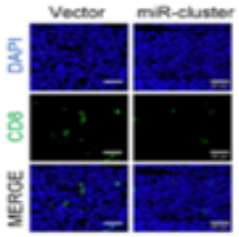

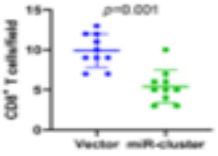

e)

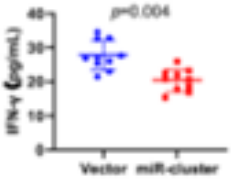

f)

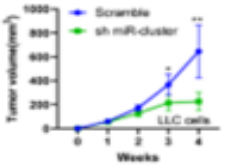

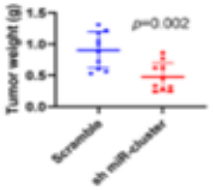

g)

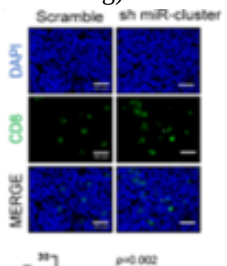

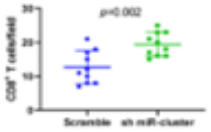

h)

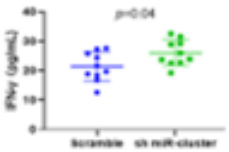

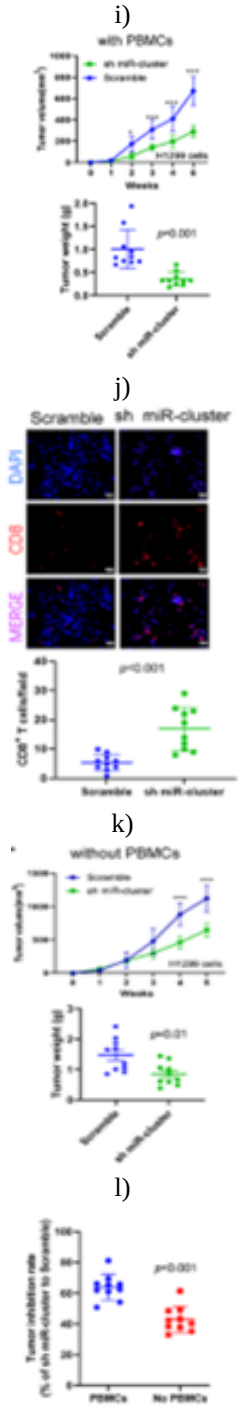

Figure 2. The miR-23a/27a/24−2 cluster suppresses T cell-mediated immune activity in NSCLC

(a) IFN-γ concentration detected in supernatants after co-culturing CD8+ T cells with NSCLC cells at a 10:1 ratio for 12 hours, (b) Quantification of CD8+ T cell-mediated killing of NSCLC cells by flow cytometry. Tumor cells expressing vector control or miR-23a/27a/24−2 cluster were incubated with activated CD8+ T cells at a 1:20 ratio for 6 hours, (c) Migration efficiency of human CD8+ T cells exposed to conditioned medium harvested from H1299 or H1650 cells transfected with control vectors or miR-23a/27a/24−2 cluster constructs, (d) Tumor volume kinetics and endpoint weights in C57BL/6J mice bearing LLC xenografts transfected with control vector or miR-23a/27a/24−2 cluster overexpression plasmids, (e) Representative immunofluorescence staining for CD8 and quantification of infiltrating CD8+ T cells (per 100 × 100 μm field) in tumors from (d) (scale bar: 50 μm; green fluorescence labels CD8+ T cells), (f) IFN-γ protein levels measured in tumor extracts from the C57BL/6J model shown in (d), (g) Tumor growth curves and weights in C57BL/6J xenografts generated with LLC cells expressing scramble control or miR-23a/27a/24−2 cluster-targeted shRNA, (h) Immunofluorescence images of CD8+ T cells and infiltration counts (100 × 100 μm area) in tumors from (g) (scale bar: 50 μm; green fluorescence indicates CD8+ T cells), (i) IFN-γ concentrations in tumor tissues from the experiment in (g), (j) Tumor growth and weights in PBMC-reconstituted SCID mice implanted with H1299 cells carrying scramble or cluster shRNA, (k) Representative CD8 immunofluorescence and infiltration quantification (100 × 100 μm area) in SCID tumors from (j) (scale bar: 50 μm; red fluorescence marks CD8+ T cells), (l) Tumor progression and final weights in non-reconstituted SCID mice using H1299 cells with scramble or cluster shRNA, and (m) Percentage tumor growth inhibition resulting from miR-23a/27a/24−2 cluster knockdown in SCID models with and without PBMC transfer (data from j and l). Each experimental group included 10 mice. In vitro assays were performed in triplicate. Values represent means ± SD. Statistical comparisons used the t-test. *, $P < 0.05$; **, $P < 0.01$; ***, $P < 0.001$ versus respective vector or scramble controls. LLC, Lewis lung cancer; IFN-γ, interferon-γ; miR-cluster, miR-23a/27a/24−2 cluster; sh miR-cluster, shRNA of miR-23a/27a/24−2 cluster; PBMCs, peripheral blood mononuclear cells.

miRNAs in the miR-23a/27a/24−2 cluster upregulated PD-L1 expression and downregulated MHC-I expression in NSCLC

To identify the molecular mediators underlying the immunosuppressive activity of the miR-23a/27a/24−2 cluster on T cell responses, a comprehensive proteomic

screen was performed in NSCLC cells engineered to express high levels of the entire cluster, compared with control cells. The analysis revealed widespread changes in protein abundance, prominently featuring increased PD-L1 and decreased MHC-I, two molecules critically involved in tumor immune escape and resistance to immune checkpoint blockade (ICB) **(Figure 3a)**. Supporting pathway analysis indicated that cluster overexpression was associated with disruption of MHC-I-dependent antigen processing and presentation **(Figure 3a)**.

Western blotting verified that the miR-23a/27a/24−2 cluster consistently elevated PD-L1 while reducing MHC-I protein expression in NSCLC cells under both unstimulated and IFN-γ-stimulated conditions **(Figure 3b)**. These alterations occurred independently of the cluster's inhibitory effect on T cell IFN-γ production. Simultaneous expression of all three cluster miRNAs exerted a more pronounced impact on PD-L1 upregulation and MHC-I downregulation than any single miRNA alone, underscoring their cooperative action. Surface expression changes were further validated by flow cytometry **(Figure 3c)** and immunofluorescence microscopy **(Figure 3d)**. Proteomic profiling aligned with these observations.

In vivo, immunohistochemical staining of tumors from LLC xenografts in C57BL/6J mice confirmed higher PD-L1 and lower MHC-I levels upon cluster overexpression **(Figure 3e)**. Similar patterns were evident in patient-derived NSCLC tissues, where tumors with high cluster miRNA expression displayed elevated PD-L1 and reduced MHC-I staining compared with low-expression cases **(Figure 3f)**. These collective findings establish that the miR-23a/27a/24−2 cluster enhances immune evasion in NSCLC through coordinated regulation of PD-L1 and MHC-I.

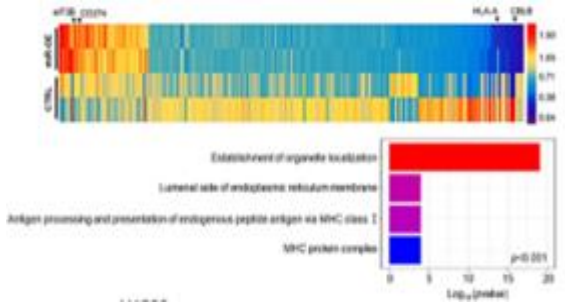

a)

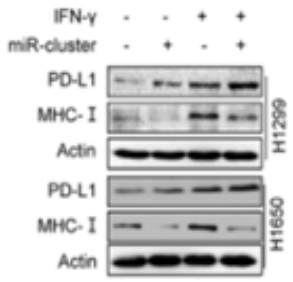

b)

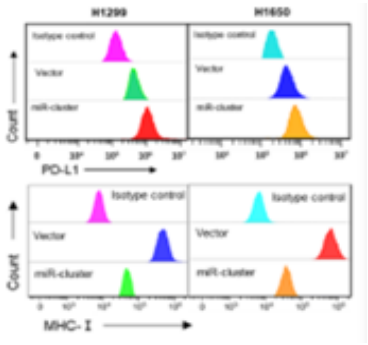

c)

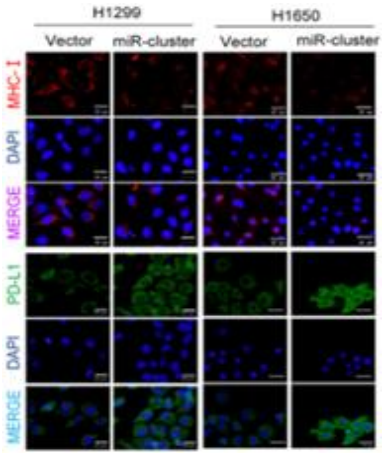

d)

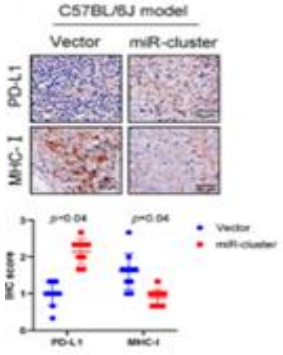

e)

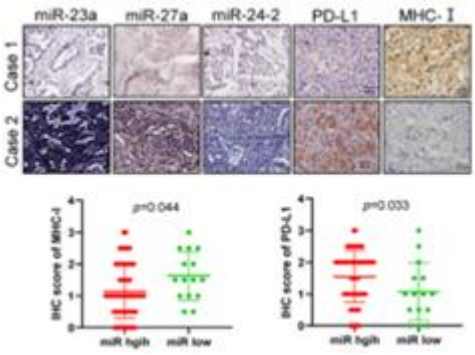

f)

Figure 3. The miR-23a/27a/24−2 cluster controls PD-L1 and MHC-I levels in NSCLC

(a) Proteomic heatmap and corresponding Gene Ontology analysis of proteins altered in H1299 cells overexpressing the miR-23a/27a/24−2 cluster relative to controls, (b) Western blot results showing increased PD-L1 and decreased MHC-I protein abundance in NSCLC cells transfected with the cluster, with or without 20 ng/ml IFN-γ for 24 hours, (c) Flow cytometric assessment and (d) immunofluorescence imaging (scale bar: 20 μm) demonstrating reduced MHC-I and elevated PD-L1 expression following cluster overexpression. Analyses were performed 72 hours after transfection. Data represent three independent experiments, (e) Typical immunohistochemical staining patterns and quantitative scores for PD-L1 and MHC-I in C57BL/6J xenograft tumors derived from experiments in **Figure 2d** (scale bar: 50 μm), and (f) Representative immunohistochemical staining and scoring of PD-L1 and MHC-I in clinical NSCLC samples from patients with high (n = 67) versus low (n = 15) miR-23a/27a/24−2 cluster expression (scale bar: 50 μm). p values were calculated using the Wilcoxon signed rank test (e) and Wilcoxon rank sum test (f). miR-cluster, miR-23a/27a/24−2 cluster; miR-OE, miR-23a/27a/24−2 cluster overexpression; CTRL, control; miR high, high expression of miRNAs in miR-23a/27a/24−2 cluster; miR low, low expression of miRNAs in miR-23a/27a/24−2 cluster.

miRNAs in the miR-23a/27a/24−2 cluster upregulated the expression of PD-L1 in NSCLC by targeting CBLB

Further investigation focused on elucidating how the miR-23a/27a/24−2 cluster governs PD-L1 abundance in NSCLC cells. Proteomics profiling revealed reduced levels of CBLB, a known PD-L1 suppressor, in cells with cluster overexpression **(Figure 3a)** [22]. This downregulation was validated at the protein level through Western blotting **(Figure 4a)** and at the transcript level by qRT-PCR **(Figure 4b)**. Ectopic expression of CBLB successfully prevented the cluster-driven elevation of PD-L1 **(Figure 4c)**, confirming that suppression of CBLB is the primary mechanism.

Computational prediction (targetscan.org) identified complementary sequences in the 3′-untranslated region (3′-UTR) of CBLB for miR-23a and miR-27a **(Figure 4d)**. Functional validation using luciferase reporters demonstrated that cluster overexpression strongly inhibited activity driven by the wild-type CBLB 3′-UTR. At the same time, mutation of the predicted binding sites abolished this repression **(Figure 4e)**. In vivo immunohistochemical studies reinforced these findings, showing an inverse relationship between cluster miRNA levels and CBLB expression, together with a positive association with PD-L1, in LLC-based C57BL/6J xenografts **(Figure 4f)** and in patient NSCLC tissues **(Figure 4g)**. These results collectively establish that the miR-23a/27a/24−2 cluster elevates PD-L1 in NSCLC by directly targeting the 3′-UTR of CBLB, thereby relieving its inhibitory action.

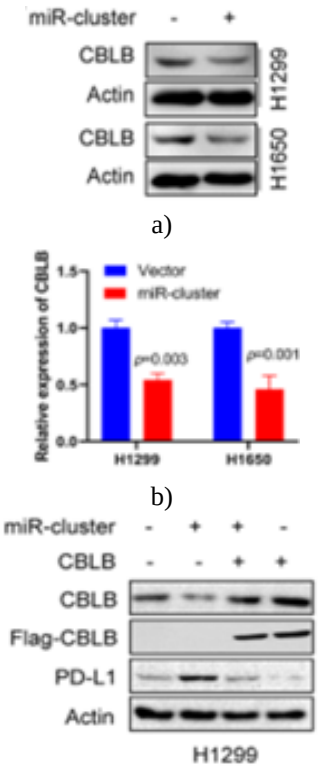

a)

b)

c)

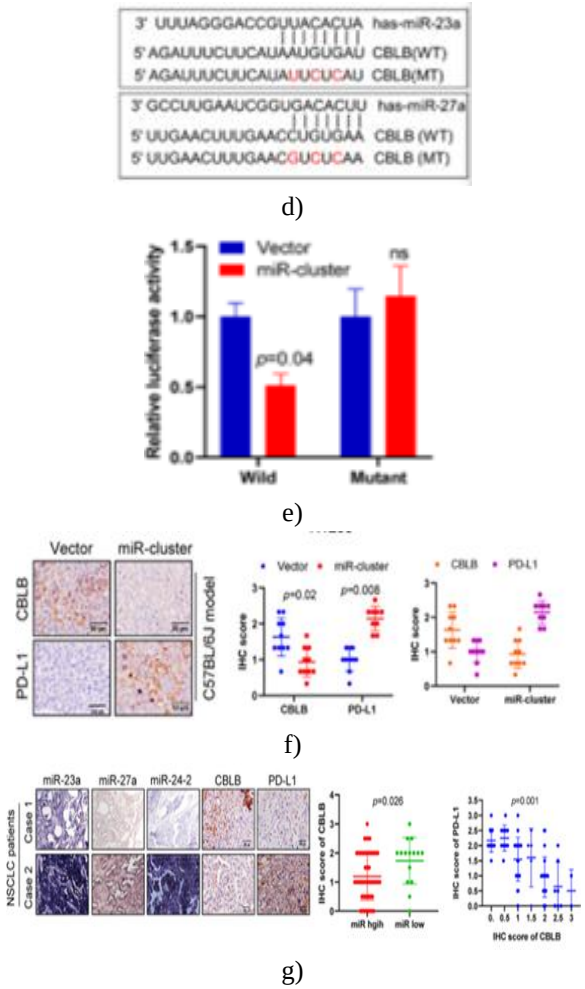

Figure 4. The miR-23a/27a/24−2 cluster elevates PD-L1 expression by targeting CBLB in NSCLC

(a) Western blot and (b) qRT-PCR results demonstrating downregulation of CBLB at protein and mRNA levels following miR-23a/27a/24−2 cluster overexpression; (c) Forced CBLB expression blocks the PD-L1 induction caused by the miR-23a/27a/24−2 cluster in H1299 cells. Transfections included the indicated vectors, cluster constructs, and/or CBLB plasmids, with analysis performed 72 hours later. Experiments (a-c) were conducted in three independent replicates, (d) Sequence complementarity between miR-23a/miR-27a and the 3′ UTR of CBLB, (E) Luciferase assay confirming that the cluster suppresses reporter activity from the wild-type CBLB 3′ UTR but not from the mutated construct, (f) Representative IHC staining and scoring for CBLB and PD-L1 in tumors from C57BL/6J xenografts (tissues sourced from **Figure 2d**; scale bar: 50 μm), and (g) IHC images and quantitative scores of CBLB and PD-L1 in human NSCLC tumors stratified by high (n = 67) or low (n = 15) miR-23a/27a/24−2 cluster expression (scale bar: 50 μm). Results are shown as means ± SD. Statistical analyses used the t-test (b and e), Wilcoxon signed rank test (f), Wilcoxon rank sum test (g-left panel), and one-way ANOVA (g-right panel). miR-cluster, miR-23a/27a/24−2 cluster; miR high, high expression of miR-23a/27a/24−2 cluster miRNAs; miR low, low expression of miR-23a/27a/24−2 cluster miRNAs.

miRNAs in the miR-23a/27a/24 − 2 cluster inhibit the expression of MHC-I in NSCLC by targeting MITF

This investigation further explored the mechanism through which the miR-23a/27a/24 − 2 cluster regulates MHC-I expression. Proteomic profiling indicated elevated eIF3B protein levels in cells overexpressing the miR-23a/27a/24 − 2 cluster **(Figure 3a)**. Bioinformatic prediction additionally identified complementary binding sequences for all three miRNAs of this cluster within the 3′-UTR of MITF **(Figure 5a)**. In line with previous reports by Santasusagna *et al*. [23], MITF acts as a repressor of eIF3B, and eIF3B itself negatively regulates MHC-I. These interactions suggest that the miR-23a/27a/24 − 2 cluster downregulates MHC-I in NSCLC cells by relieving MITF-mediated suppression of eIF3B. Consistent with this model, enforced expression of the miR-23a/27a/24 − 2 cluster strongly decreased MITF and MHC-I protein abundance while simultaneously increasing eIF3B levels in NSCLC cell lines **(Figure 5b)**. Parallel qRT-PCR experiments confirmed that the cluster also reduced MITF transcript levels **(Figure 5c)**. Rescue experiments demonstrated that restoring MITF expression or depleting eIF3B effectively reversed the MHC-I downregulation caused by the miR-23a/27a/24 − 2 cluster **(Figure 5d)**. Moreover, MITF overexpression prevented the cluster-dependent induction of eIF3B **(Figure 5d)**. To confirm direct targeting, luciferase reporter constructs containing either the wild-type or mutated 3′-UTR of MITF were employed. Overexpression of the miR-23a/27a/24 − 2 cluster significantly reduced luciferase activity from the wild-type reporter but had no impact on the mutant version **(Figure 5e)**. In vivo and clinical validation was obtained through immunohistochemical analysis of xenograft tumors derived from miR-23a/27a/24 − 2 cluster-overexpressing LLC cells in C57BL/6J mice **(Figure 5f)** as well as primary tumor specimens from NSCLC patients stratified by miR-23a/27a/24 − 2 cluster expression **(Figure 5g)**. Overall, these data establish that miRNAs of the miR-23a/27a/24 − 2 cluster inhibit

MHC-I expression in non-small cell lung cancer by directly targeting MITF, thereby upregulating eIF3B.

a)

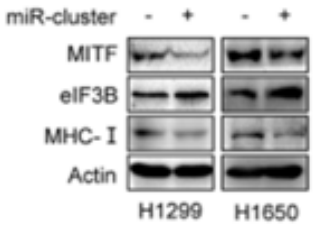

b)

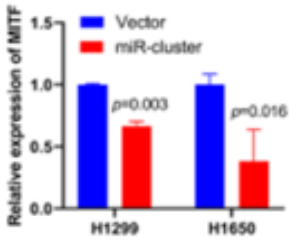

c)

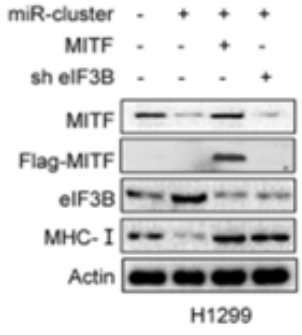

d)

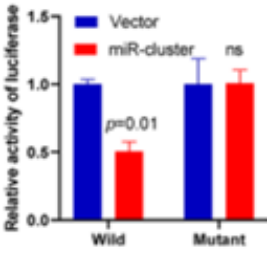

e)

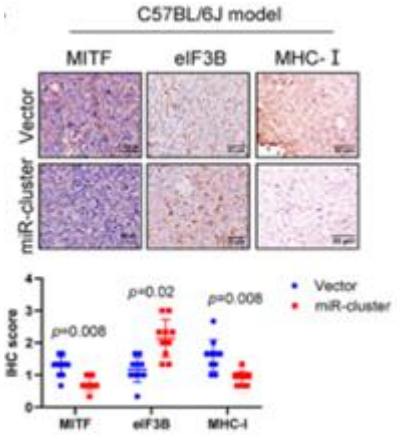

f)

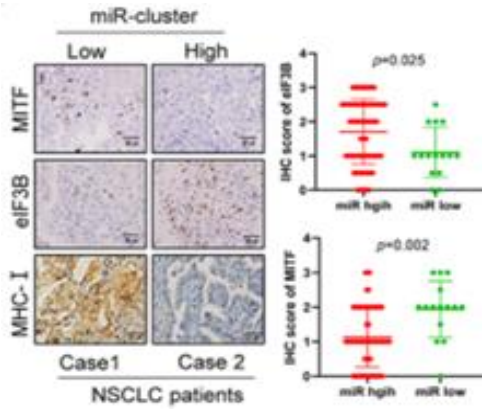

g)

Figure 5. The miR-23a/27a/24 − 2 cluster suppressed MHC-I expression through the MITF/eIF3B axis in NSCLC

(a) Sequence alignment showing complementarity between miRNAs of the miR-23a/27a/24 − 2 cluster and the 3′-UTR of MITF, (b) Western blot analysis demonstrated that overexpression of the miR-23a/27a/24 − 2 cluster reduced MITF and MHC-I protein levels while elevating eIF3B in NSCLC cells, (c) qRT-PCR analysis revealed that overexpression of the miR-23a/27a/24 − 2 cluster decreased MITF mRNA expression in NSCLC cells, (d) Western blot analysis indicated that the miR-23a/27a/24 − 2 cluster-mediated suppression of MHC-I could be rescued by MITF overexpression or eIF3B knockdown in H1299 cells. The indicated NSCLC cells were transfected with the corresponding constructs. Cells were analyzed 72 h post-transfection. Data represent three independent in vitro experiments (B-D), (e) Luciferase reporter assay showing that the miR-23a/27a/24 − 2 cluster inhibited luciferase activity driven by the wild-type 3′ UTR of MITF in NSCLC cells, without influencing the mutated

3′ UTR construct, (f) Representative immunohistochemical (IHC) staining and quantitative scores for MITF, eIF3B, and MHC-I in C57BL/6J xenograft tumors. Tumor tissues were obtained from **Figure 2d** (scale bar: 50 μm), and (g) Representative IHC images and scoring of MITF, eIF3B, and MHC-I in tumor samples from NSCLC patients exhibiting high (n = 67) or low (n = 15) expression of the miR-23a/27a/24 − 2 cluster (scale bar: 50 μm). Data are presented as means ± SD. Statistical significance was determined by Student's t-test (c and d), Wilcoxon signed rank test (f), and Wilcoxon rank sum test (g). miR-cluster, miR-23a/27a/24 − 2 cluster; miR high, high expression of miR-23a/27a/24 − 2 cluster miRNAs; miR low, low expression of miR-23a/27a/24 − 2 cluster miRNAs.

miRNAs in the miR-23a/27a/24 − 2 cluster maintain their expression through the β-catenin/TCF4 axis in NSCLC

To clarify the mechanism controlling the miR-23a/27a/24 − 2 cluster in NSCLC, potential transcription factors capable of regulating its expression were systematically evaluated. This screening process revealed that TCF4 binds to the promoter of the miR-23a/27a/24 − 2 cluster **(Figure 6a)**. As a critical downstream mediator of Wnt/β-catenin signaling, TCF4 participates in miRNA transcriptional control by associating with miRNA promoter elements [24]. Earlier findings from our group indicated that the miRNAs of the miR-23a/27a/24 − 2 cluster enhance the transcriptional output of the TCF/LEF complex by stimulating Wnt/β-catenin pathway activity in NSCLC [9]. These observations led to the hypothesis that the miR-23a/27a/24 − 2 cluster perpetuates its own expression via a β-catenin/TCF4-dependent positive feedback circuit. The initial experimental validation confirmed TCF4's regulatory role in the cluster. Ectopic expression of TCF4 markedly increased the levels of miR-23a, miR-27a, and miR-24-2 **(Figure 6b)**. It boosted promoter activity as measured by luciferase reporter assays **(Figure 6c)**. Electrophoretic mobility shift assay (EMSA) further established that TCF4 physically interacts with the specific binding motif in the miR-23a/27a/24 − 2 cluster promoter; alteration of this motif substantially weakened the binding **(Figure 6d)**. Taken together, these data show that TCF4 directly activates transcription of the miR-23a/27a/24 − 2 cluster miRNAs. Additional studies examined the contribution of β-catenin to this process. Overexpression of β-catenin enhanced the occupancy of TCF4 at the miR-23a/27a/24 − 2 cluster promoter **(Figures 6e and 6f)**, augmented promoter-driven luciferase activity **(Figure 6g)**, and elevated the expression of the cluster miRNAs **(Figure 6h)**. Treatment with the small-molecule inhibitor LF3, which interferes with β-catenin–TCF4 complex formation, potently abrogated the upregulation of miR-23a/27a/24 − 2 cluster miRNAs triggered by β-catenin overexpression **(Figure 6i)**. In conclusion, these results demonstrate that the miR-23a/27a/24 − 2 cluster sustains its expression in NSCLC cells through an autoregulatory loop driven by the β-catenin/TCF4 signaling axis.

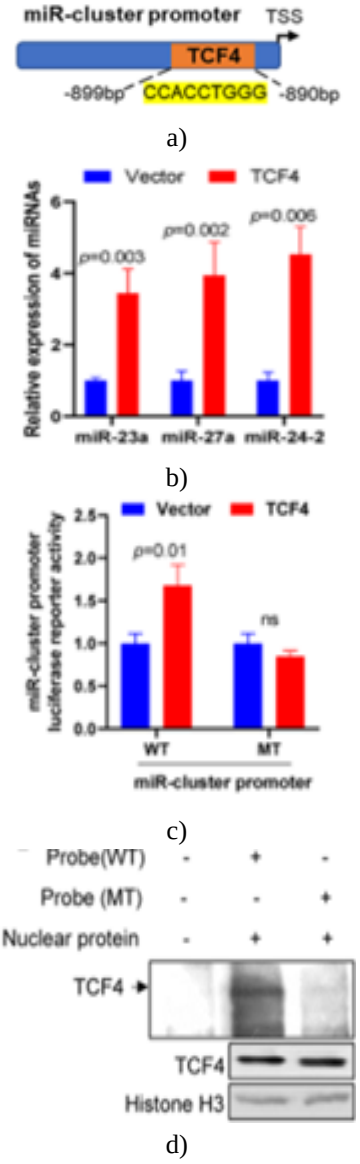

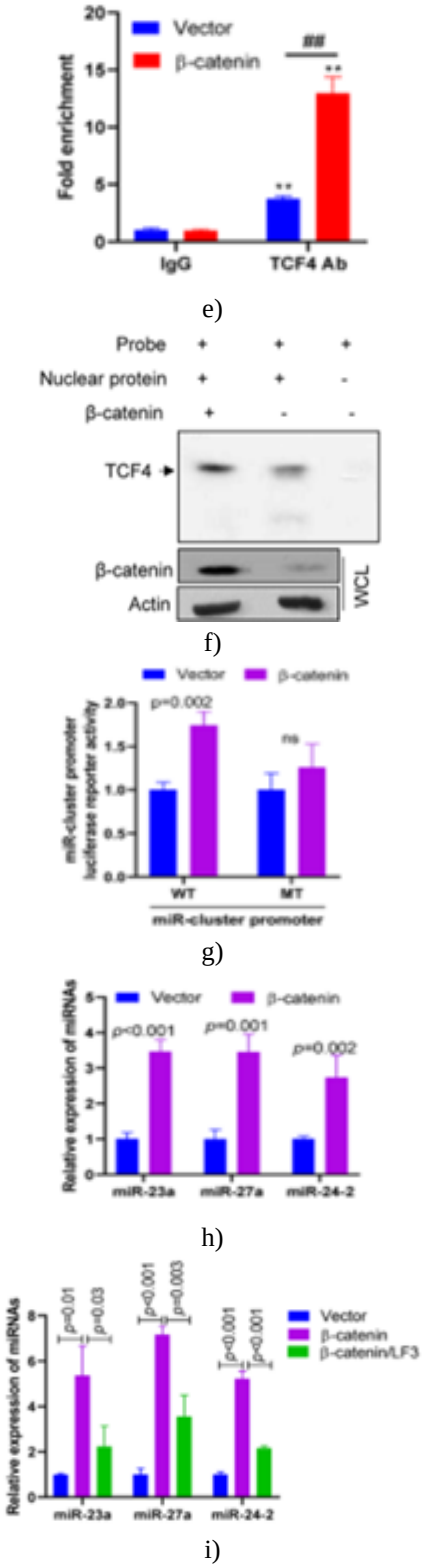

Figure 6. The miR-23a/27a/24 − 2 cluster maintains its expression through the β-catenin/TCF4 axis in NSCLC

(a) Identification of potential TCF4-binding sequences located in the promoter region of the miR-23a/27a/24 − 2 cluster, (b) qRT-PCR analysis demonstrated that TCF4 overexpression upregulated the expression of miR-23a, miR-27a, and miR-24-2 in 293T cells, (c) Luciferase reporter assay showed that TCF4 overexpression enhanced luciferase activity controlled by the wild-type promoter of the miR-23a/27a/24 − 2 cluster in 293T cells, (d) EMSA confirmed the physical interaction between TCF4 and the miR-23a/27a/24 − 2 cluster promoter in 293T cells, (e) ChIP-qPCR results showing that β-catenin overexpression promoted the recruitment of TCF4 to the miR-23a/27a/24 − 2 cluster promoter in 293T cells. **, $p < 0.01$ compared to Vector control (IgG); ##, $p < 0.01$ compared to Vector control (TCF4 Ab), (f) EMSA showing that β-catenin overexpression strengthened the binding of TCF4 to the miR-23a/27a/24 − 2 cluster promoter in 293T cells, (g) Luciferase reporter assay demonstrating that β-catenin overexpression increased luciferase expression driven by the wild-type promoter of the miR-23a/27a/24 − 2 cluster in 293T cells, without affecting the mutated promoter construct, (h) qRT-PCR analysis showed that β-catenin overexpression elevated the expression of all miRNAs belonging to the miR-23a/27a/24 − 2 cluster, and (i) qRT-PCR analysis showed that pharmacological inhibition of the β-catenin–TCF4 interaction by 30 μm LF3 (6 h treatment) attenuated β-catenin-induced upregulation of miR-23a/27a/24 − 2 cluster miRNAs in 293T cells. 293T cells were transfected with the indicated constructs for 72 h and then analyzed (B-H). Data are presented as means ± SD. p-values were calculated by t-test (B, C, G and H) or one-way ANOVA followed by Duncan's multiple range test (E and I). miR-cluster, miR-23a/27a/24 − 2 cluster; ns, no significance; WT, wild type; MT, mutant; WCL, whole cell lysate.

Targeting the eIF3B pathway dramatically enhances the therapeutic efficacy of PD-1/PD-L1 blockade in lung cancers with high expression of miRNAs in the miR-23a/27a/24−2 cluster

Because the miR-23a/27a/24−2 cluster regulates several molecules central to the success of PD-1/PD-L1 blockade, we assessed whether elevated expression of these miRNAs promotes resistance to this therapeutic approach. Consistent with expectations, forced expression of the cluster miRNAs decreased tumor sensitivity to PD-L1 monoclonal antibody administration **(Figure 7a)** and limited CD8+ T cell

recruitment into neoplastic lesions in C57BL/6J mice harboring LLC xenografts **(Figure 7b)**.

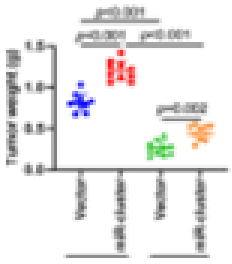

a)

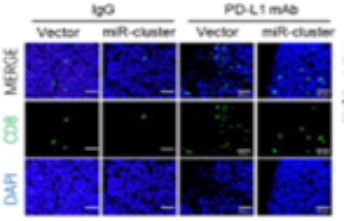

b)

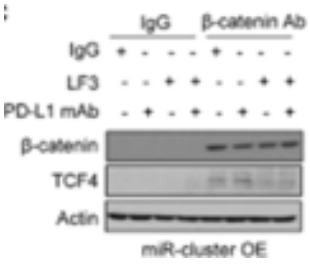

c)

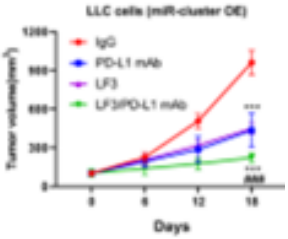

d)

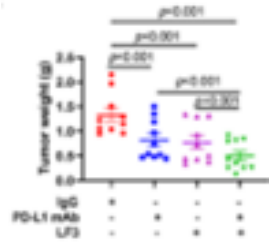

e)

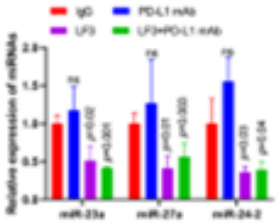

f)

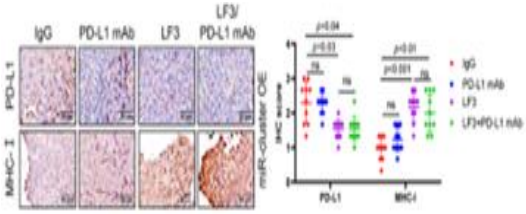

g)

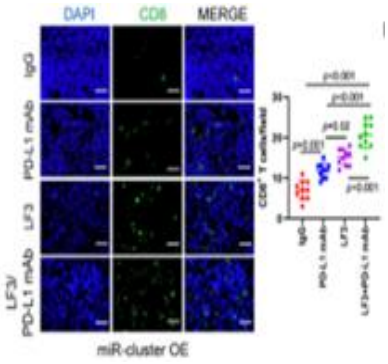

h)

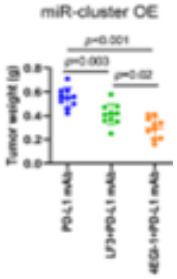

i)

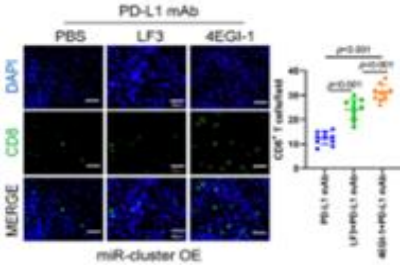

j)

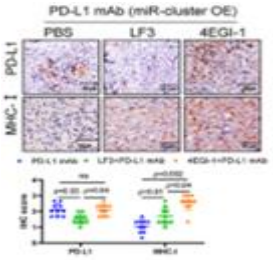

k)

Figure 7. Pharmacological inhibition of eIF3B reverses miR-23a/27a/24−2 cluster-driven resistance to immune checkpoint blockade in C57BL/6J xenograft models established with LLC cells

(a) Final tumor weights of control vector or miR-23a/27a/24−2 cluster-overexpressing LLC tumors in C57BL/6J mice receiving IgG or PD-L1 mAb, (b) Representative immunofluorescence staining for CD8+ T cells and quantification of tumor-infiltrating CD8+ T cells (per 100 × 100 μm field; scale bar: 50 μm) in tissues from (a), (c) Co-immunoprecipitation assay indicating that LF3 treatment disrupts β-catenin binding to TCF4 in xenograft tumors. Tissues collected from experiments shown in (d), (d) Tumor growth kinetics, (e) endpoint tumor weights, and (f) expression levels of miR-23a/27a/24−2 cluster miRNAs in C57BL/6J xenografts treated with the specified therapeutic agents. Models used LLC cells overexpressing the miR-23a/27a/24−2 cluster. Treatment commenced once mean tumor volume reached approximately 100 mm^3. (g) Representative immunohistochemical staining and scoring for PD-L1 and MHC-I across treatment groups (scale bar: 50 μm). Tissues from (d), (h) Representative immunofluorescence images of CD8+ T cells and corresponding infiltration counts (100 × 100 μm area) in tumors from the different treatment arms (scale bar: 50 μm). Tissues from (d), (i) Tumor weights, (j) representative immunofluorescence staining for CD8+ T cells (scale bar: 50 μm) with infiltration quantification (100 × 100 μm area), and (k) representative immunohistochemical staining (scale bar: 50 μm) with scoring of PD-L1 and MHC-I in tumors from mice receiving the indicated treatments. High miR-23a/27a/24−2 cluster-expressing LLC xenografts in C57BL/6J mice were treated starting at ~100 mm^3 tumor volume. Tumors were harvested 18 days after treatment initiation for analyses (c-k). Each experimental group included 10 mice. Data represent means ± SD. Statistical comparisons used one-way ANOVA followed by Duncan's multiple range test (A, B, D, E, F, H, I and J) and Kruskal-Wallis test with Dunn's post-hoc test (G and K). miR-cluster, miR-23a/27a/24−2 cluster; miR-cluster OE, overexpression of miR-23a/27a/24−2 cluster; PD-L1 mAb, PD-L1 monoclonal antibody; ***, $p < 0.001$ versus IgG group; ###, $p < 0.001$ versus single-agent groups.

Earlier reports have identified hyperactivation of the β-catenin pathway [25] and the eIF3B/MHC-I axis [23] as important drivers of resistance to PD-1/PD-L1 inhibitors. Considering that high miR-23a/27a/24−2 cluster expression promotes such resistance, maintains itself via β-catenin/TCF4 signaling, and attenuates MHC-I through eIF3B, we tested whether pharmacological interference with these pathways could sensitize cluster-high tumors to PD-1/PD-L1 blockade.

Animal studies demonstrated that LF3, which blocks β-catenin/TCF4 association **(Figure 7c)**, substantially retarded growth of cluster-overexpressing tumors compared with vehicle-treated controls **(Figures 7d and 7e)**. The combination of LF3 with PD-L1 mAb yielded greater antitumor activity than monotherapy with either agent **(Figures 7d and 7e)**. LF3 administration also reduced cluster miRNA levels **(Figure 7f)**, decreased PD-L1 expression, and increased MHC-I expression **(Figure 7g)**. The dual treatment further promoted robust infiltration of CD8+ T cells into the tumor bed **(Figure 7h)**.

Direct comparison revealed that inhibition of the eIF3B pathway using 4EGI-1, which prevents eIF3B participation in translation initiation and interrupts MITF/eIF3B signaling [23, 26], produced superior enhancement of PD-L1 mAb efficacy in cluster-high tumors than LF3-mediated β-catenin/TCF4 blockade **(Figure 7i)**. The 4EGI-1/PD-L1 mAb combination also resulted in greater CD8+ T cell accumulation within tumors **(Figure 7j)**. Importantly, 4EGI-1 restored MHC-I levels without interfering with the cluster-induced elevation of PD-L1 **(Figure 7k)**. In aggregate, these observations highlight that pharmacological targeting of eIF3B offers a particularly effective means to overcome resistance and improve the outcomes of PD-1/PD-L1 blockade therapy in lung cancers with high expression of the miR-23a/27a/24−2 cluster.

The current investigation delineates the molecular mechanisms by which miRNAs of the miR-23a/27a/24−2 cluster drive immune evasion and confer resistance to PD-1/PD-L1 inhibitors in non-small cell lung cancer (NSCLC). Extensive literature has

established PD-L1 [27] and MHC-I [28] as central mediators of tumor-immune interactions. PD-L1 acts as a checkpoint ligand on tumor cells, binding to PD-1 on T lymphocytes and thereby attenuating their effector functions. Consequently, excessive PD-L1 production enables malignant cells to evade immune attack. Likewise, reduced MHC-I levels represent a common immune escape strategy. MHC-I complexes present antigenic peptides on cell surfaces, alerting the immune system to the presence of abnormal cells [29]. Recognition of tumor-derived peptides by CD8+ T cells triggers their activation and subsequent cytotoxic destruction of cancer cells [29]. However, downregulation or complete loss of MHC-I frequently occurs in lung cancer and other malignancies [30, 31], allowing tumors to escape T cell recognition and persist [31].

Our findings demonstrate that elevated expression of the miR-23a/27a/24−2 cluster facilitates immune evasion and impairs responsiveness to PD-1/PD-L1 blockade in NSCLC. Mechanistically, these miRNAs enhance PD-L1 production by suppressing the negative regulator CBLB and attenuate MHC-I levels by increasing the negative regulator eIF3B through direct inhibition of MITF. Supporting this role, components of the cluster have been implicated in immune suppression in other cancer types. For example, miR-27a reduces MHC-I surface expression and restricts CD8+ T cell infiltration in colorectal carcinoma [28]. Lin *et al*. [32] showed that miR-23a upregulation in CD8+ cytotoxic T cells promotes tumor-mediated immunosuppression in lung cancer, and its inhibition can reverse this phenotype. In addition, increased miR-23a and miR-27a in tumor-associated macrophages elevate PD-L1 via the PTEN/PIK3 axis in hepatocellular carcinoma [33] and breast cancer [34], respectively. Together, these lines of evidence indicate that the miR-23a/27a/24−2 cluster promotes tumor immune escape by coordinately increasing PD-L1 and decreasing MHC-I. The present work uncovers a distinct regulatory pathway responsible for these alterations in NSCLC.

We have also clarified how the miR-23a/27a/24−2 cluster sustains its abnormally high expression in NSCLC. Although this cluster is overexpressed in nearly half of early-stage NSCLC cases and strongly associates with aggressive disease [9], the basis for its persistent upregulation was previously unclear. We now show that TCF4 binds the cluster promoter to drive transcription, and β-catenin enhances this binding. When integrated with our earlier demonstration that the cluster activates Wnt/β-catenin signaling and potentiates TCF/LEF-mediated gene expression by targeting pathway inhibitors [9], these results reveal a self-reinforcing positive feedback mechanism. Accordingly, the miR-23a/27a/24−2 cluster maintains high expression levels through continuous stimulation of the β-catenin/TCF4 axis. Interrupting this loop therefore emerges as a rational strategy for managing tumors with strong cluster activity. Consistent with this notion, our previous research showed that suppressing either the cluster or β-catenin effectively restrains tumor growth in high-cluster NSCLC [9].

Lastly, we identify a promising intervention for NSCLC with high expression of the miR-23a/27a/24−2 cluster. The cluster stimulates both β-catenin signaling [9] and the eIF3B pathway, each of which has been linked to PD-1/PD-L1 blockade resistance [23, 35]. Our experiments reveal that pharmacological disruption of either the β-catenin/TCF4 interaction or the eIF3B pathway markedly improves the efficacy of PD-L1 monoclonal antibody therapy. Notably, eIF3B inhibition yielded greater sensitization than β-catenin/TCF4 blockade. This differential benefit may arise from their opposing influences on PD-L1 and MHC-I. Clinical data emphasize that PD-1/PD-L1 blockade outcomes correlate closely with tumor PD-L1 levels [36, 37], and in some contexts elevated PD-L1 can improve therapeutic responses [38]. At the same time, β-catenin/TCF4 inhibition restored MHC-I but lowered PD-L1, and eIF3B targeting preserved cluster-driven PD-L1 elevation while strongly upregulating MHC-I.

Conclusion

Taken together, miRNAs of the miR-23a/27a/24−2 cluster perpetuate their expression in NSCLC through activation of the β-catenin/TCF4 signaling cascade. High cluster activity elevates PD-L1 by inhibiting its negative regulator CBLB, and reduces MHC-I by increasing eIF3B following direct MITF suppression **(Figure 8)**, (left). Furthermore, this study introduces an effective treatment approach whereby inhibition of the eIF3B pathway substantially potentiates PD-1/PD-L1 blockade in cluster-high lung cancers. This sensitization occurs through restoration of MHC-I expression while preserving the high PD-L1 levels induced by the miR-23a/27a/24−2 cluster **(Figure 8)**, (right).

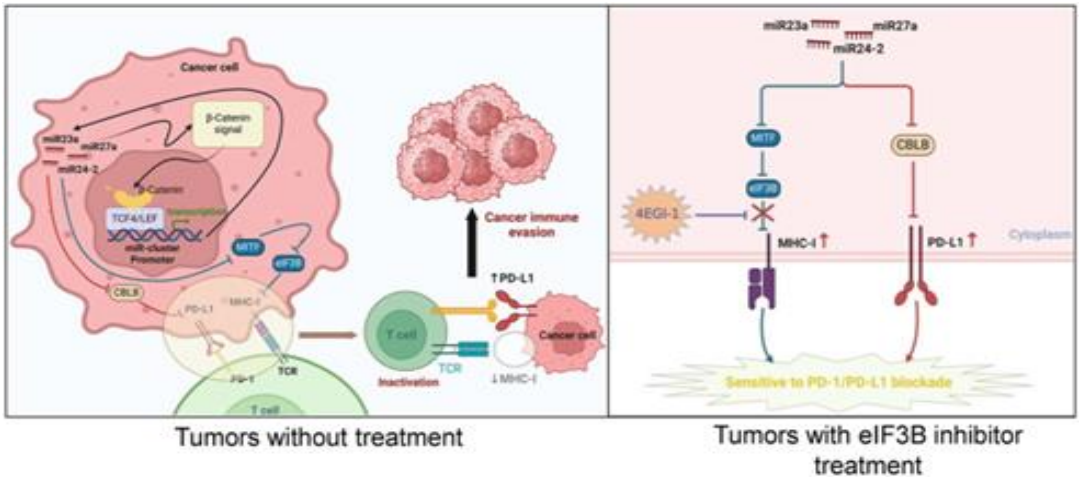

Figure 8. Schematic representations depicting how miRNAs of the miR-23a/27a/24−2 cluster sustain their own expression and facilitate tumor immune evasion (left), and how eIF3B inhibition sensitizes high miR-23a/27a/24−2 cluster-expressing tumors to PD-1/PD-L1 blockade (right).

Acknowledgments: None

Conflict of Interest: None

Financial Support: None

Ethics Statement: None

References

1. Bray F, Laversanne M, Sung H, Ferlay J, Siegel RL, Soerjomataram I, et al. Global cancer statistics 2022: GLOBOCAN estimates of incidence and mortality worldwide for 36 cancers in 185 countries. CA Cancer J Clin. 2024;74(3):229–63.
2. Cronin KA, Lake AJ, Scott S, Sherman RL, Noone AM, Howlader N, et al. Annual Report to the Nation on the Status of Cancer, part I: National cancer statistics. Cancer. 2018;124(13):2785–800.
3. Zavitsanou AM, Pillai R, Hao Y, Wu WL, Bartnicki E, Karakousi T, et al. KEAP1 mutation in lung adenocarcinoma promotes immune evasion and immunotherapy resistance. Cell Rep. 2023;42(11):113295.
4. Vinay DS, Ryan EP, Pawelec G, Talib WH, Stagg J, Elkord E, et al. Immune evasion in cancer: mechanistic basis and therapeutic strategies. Semin Cancer Biol. 2015;35:S185–98.
5. Cable J, Greenbaum B, Pe'er D, Bollard CM, Bruni S, Griffin ME, et al. Frontiers in cancer immunotherapy-a symposium report. Ann N Y Acad Sci. 2021;1489(1):30–47.
6. Sharma P, Hu-Lieskovan S, Wargo JA, Ribas A. Primary, adaptive, and acquired resistance to cancer immunotherapy. Cell. 2017;168(4):707–23.
7. Cioffi M, Trabulo SM, Vallespinos M, Raj D, Kheir TB, Lin ML, et al. The miR-25-93-106b cluster regulates tumor metastasis and immune evasion via modulation of CXCL12 and PD-L1. Oncotarget. 2017;8(13):21609–25.
8. Kundu ST, Rodriguez BL, Gibson LA, Warner AN, Perez MG, Bajaj R, et al. The microRNA-183/96/182 cluster inhibits lung cancer progression and metastasis by inducing an interleukin-2-mediated antitumor CD8 cytotoxic T-cell response. Genes Dev. 2022;36(9–10):582–600.
9. Fan XQ, Tao SL, Li Q, Deng B, Tan QY, Jin H. The miR-23a/27a/24–2 cluster promotes postoperative progression of early-stage non-small cell lung cancer. Mol Ther Oncolytics. 2022;24:205–17.
10. Muto S, Enta A, Maruya Y, Inomata S, Yamaguchi H, Mine H, et al. Wnt/β-Catenin signaling and resistance to immune checkpoint inhibitors: from non-small-cell lung cancer to other cancers. Biomedicines. 2023;11(1):190.
11. Chandran PA, Keller A, Weinmann L, Seida AA, Braun M, Andreev K, et al. The TGF-β-inducible miR-23a cluster attenuates IFN-γ levels and antigen-specific cytotoxicity in human CD8 T cells. J Leukoc Biol. 2014;96(4):633–45.
12. Li Q, Zhou ZW, Lu J, Luo H, Wang SN, Peng Y, et al. PD-L1P146R is prognostic and a negative

predictor of response to immunotherapy in gastric cancer. Mol Ther. 2022;30(2):621–31.
13. Shang S, Yang YW, Chen F, Yu L, Shen SH, Li K, et al. TRIB3 reduces CD8 T cell infiltration and induces immune evasion by repressing the STAT1-CXCL10 axis in colorectal cancer. Sci Transl Med. 2022;14(626):eabf0992.
14. Li Q, Zhou ZW, Duan W, Qian CY, Wang SN, Deng MS, et al. Inhibiting the redox function of APE1 suppresses cervical cancer metastasis via disengagement of ZEB1 from E-cadherin in EMT. J Exp Clin Cancer Res. 2021;40(1):220.
15. Nuovo GJ. In situ detection of microRNAs in paraffin embedded, formalin fixed tissues and the co-localization of their putative targets. Methods. 2010;52(4):307–15.
16. Guo ZY, Hardin H, Montemayor-Garcia C, Asioli S, Righi A, Maletta F, et al. In situ hybridization analysis of miR-146b-5p and miR-21 in thyroid nodules: diagnostic implications. Endocr Pathol. 2015;26(2):157–63.
17. Li JW, Jiang HM, Lv ZY, Sun ZY, Cheng CQ, Tan GH, et al. Articular fibrocartilage-targeted therapy by microtubule stabilization. Sci Adv. 2022;8(46):eabn8420.
18. Dai FQ, Li CR, Fan XQ, Tan L, Wang RT, Jin H. Mir-150-5p inhibits non-small-cell lung cancer metastasis and recurrence by targeting HMGA2 and β-Catenin signaling. Mol Ther Nucleic Acids. 2019;16:675–85.
19. Zhang Q, Liu W, Zhang HM, Xie GY, Miao YR, Xia MX, et al. hTFtarget: a comprehensive database for regulations of human transcription factors and their targets. Genom Proteom Bioinf. 2020;18(2):120–8.
20. Vlachos IS, Zagganas K, Paraskevopoulou MD, Georgakilas G, Karagkouni D, Vergoulis T, et al. DIANA-miRPath v3.0: deciphering microRNA function with experimental support. Nucleic Acids Res. 2015;43(W1):W460–6.
21. Liu ZC, Wang TT, She YL, Wu KQ, Gu SR, Li L, et al. N-methyladenosine-modified circIGF2BP3 inhibits CD8 T-cell responses to facilitate tumor immune evasion by promoting the deubiquitination of PD-L1 in non-small cell lung cancer. Mol Cancer. 2021;20(1):105.
22. Wang S, Xu L, Che XF, Li C, Xu L, Hou KZ, et al. E3 ubiquitin ligases Cbl-b and c-Cbl downregulate PD-L1 in wild-type non-small cell lung cancer. FEBS Lett. 2018;592(4):621–30.
23. Santasusagna S, Zhu S, Jawalagatti V, Carceles-Cordon M, Ertel A, Garcia-Longarte S, et al. Master transcription factor reprogramming unleashes selective translation promoting castration resistance and immune evasion in lethal prostate cancer. Cancer Discov. 2023;13(12):2584–609.
24. Rambow F, Bechadergue A, Luciani F, Gros G, Domingues M, Bonaventure J, et al. Regulation of melanoma progression through the TCF4/miR-125b/NEDD9 cascade. J Invest Dermatol. 2016;136(6):1229–37.
25. de Galarreta MR, Bresnahan E, Molina-Sánchez P, Lindblad KE, Maier B, Sia D, et al. β-Catenin activation promotes immune escape and resistance to anti-PD-1 therapy in hepatocellular carcinoma. Cancer Discov. 2019;9(8):1124–41.
26. Moerke NJ, Aktas H, Chen H, Cantel S, Reibarkh MY, Fahmy A, et al. Small-molecule inhibition of the interaction between the translation initiation factors eIF4E and eIF4G. Cell. 2007;128(2):257–67.
27. Wang J, Ge JS, Wang YA, Xiong F, Guo JY, Jiang XJ, et al. EBV miRNAs BART11 and BART17-3p promote immune escape through the enhancer-mediated transcription of PD-L1. Nat Commun. 2022;13(1):866.
28. Colangelo T, Polcaro G, Ziccardi P, Pucci B, Muccillo L, Galgani M, et al. Proteomic screening identifies calreticulin as a miR-27a direct target repressing MHC class I cell surface exposure in colorectal cancer. Cell Death Dis. 2016;7(2):e2120.
29. Wu XY, Li TH, Jiang R, Yang X, Guo HQ, Yang R. Targeting MHC-I molecules for cancer: function, mechanism, and therapeutic prospects. Mol Cancer. 2023;22(1):194.
30. Korkolopoulou P, Kaklamanis L, Pezzella F, Harris AL, Gatter KC. Loss of antigen-presenting molecules (MHC class I and TAP-1) in lung cancer. Br J Cancer. 1996;73(2):148–53.
31. Dhatchinamoorthy K, Colbert JD, Rock KL. Cancer immune evasion through loss of MHC class I antigen presentation. Front Immunol. 2021;12:636568.
32. Lin R, Chen L, Chen G, Hu CY, Jiang S, Sevilla J, et al. Targeting miR-23a in CD8 cytotoxic T lymphocytes prevents tumor-dependent immunosuppression. J Clin Invest. 2014;124(12):5352–67.
33. Liu JT, Fan LL, Yu HQ, Zhang J, He Y, Feng DC, et al. Endoplasmic reticulum stress causes liver cancer cells to release exosomal miR-23a-3p and up-

regulate programmed death ligand 1 expression in macrophages. Hepatology. 2019;70(1):241–58.
34. Yao XL, Tu Y, Xu YL, Guo YY, Yao F, Zhang XH. Endoplasmic reticulum stress-induced exosomal miR-27a-3p promotes immune escape in breast cancer via regulating PD-L1 expression in macrophages. J Cell Mol Med. 2020;24(17):9560–73.
35. Luke JJ, Bao RY, Sweis RF, Spranger S, Gajewski TF. WNT/β-catenin pathway activation correlates with immune exclusion across human cancers. Clin Cancer Res. 2019;25(10):3074–83.
36. Herbst RS, Soria JC, Kowanetz M, Fine GD, Hamid O, Gordon MS, et al. Predictive correlates of response to the anti-PD-L1 antibody MPDL3280A in cancer patients. Nature. 2014;515(7528):563–7.
37. Iwai Y, Ishida M, Tanaka Y, Okazaki T, Honjo T, Minato N. Involvement of PD-L1 on tumor cells in the escape from host immune system and tumor immunotherapy by PD-L1 blockade. Proc Natl Acad Sci USA. 2002;99(19):12293–7.
38. Zhang JF, Bu X, Wang HZ, Zhu YS, Geng Y, Nihira NT, et al. Cyclin D-CDK4 kinase destabilizes PD-L1 via cullin 3-SPOP to control cancer immune surveillance. Nature. 2018;553(7686):91–5.